Chaotic Bursting in Single Neurons

Jon Newman*
Department of Bioengineering
Georgia Institute of Technology,
Atlanta, GA 30332-0430, U.S.A
(Dated: December 7, 2008)

It has become fashionable to report on the existence of deterministic chaos in biophysical neuron models. Much of the time, the importance of this behavior is given as self-evident. Moreover, it is rarely transparent whether these studies actually investigate a chaotic behavior since a full mathematical analysis is not pursued. This report revisits a biophysical paper reporting chaotic bursting in an intrinsically bursting neuron model ref. [1]. Using cycle-expansion techniques, we determine whether these models in fact produce chaotic oscillations and how these oscillations come to be. We related these results to biological mechanisms that may be responsible for the chaotic dynamics in neurons. Finally, we investigate how likely chaotic bursting is to play a functional role in single neurons given the presence of large noise in the vast majority of biological systems.

PACS numbers: 87.19.*ll*, 05.45.Ac, 05.10.–a
Keywords: neuronal bursting, chaos, cycle-expansions

0. DISCLAIMER

This is a term report for the class 'Chaos and What To Do About It' taught by Predrag Cvitanović at the Georgia Institute of Technology during the Fall semester of 2008. The content has not passed any rigorous peer review and may contain errors.

I. INTRODUCTION

There is little doubt that chaotic oscillations abound in neural systems. After all, even the smallest nervous systems are composed of thousands of coupled oscillators that are highly non-linear, but obviously bounded to some functional regime. Many studies, however, claim that functional chaos arises in single neurons that exhibit 'bursting' behavior ref. [1, 2]. Here we examine why this claim is true, and why it is probably meaningless.

Bursting is a dynamic state characterized by alternating periods of activity and quiescence. Many dynamical systems demonstrate bursting behavior. For instance, nerve cells can exhibit autonomous or induced bursting by firing separated groups of action potentials in time. Autonomous bursting neurons are found in a variety of neural systems, from the mammalian cortex ref. [3] and brainstem ref. [4] to identified invertebrate neurons ref. [5].

*Electronic address: jnewman6@gatech.edu

II. STATE SPACE ANALYSIS OF BURSTING

Dynamical bursting models are a system of ordinary differential equations of the form

$$\dot{x} = f(x, y), \tag{1}$$
$$\dot{y} = \epsilon g(x, y), \quad x \in \mathbb{R}^m, \quad y \in \mathbb{R}^n, \tag{2}$$

where $0 \leq \epsilon$ is a small parameter. (1–2) are singularly perturbed (SP) differential equations. Thus, using geometric singular perturbation methods ref. [1], the dynamics of bursting models can be explored by decomposing the full system into fast- and slow-subsystems: (1) and (2), respectively. Here, the slow-subsystem can act independently, be affected synaptically, or interact locally with the spiking fast-subsystem to produce alternating periods of spiking and silence in time. To examine the dynamical mechanism implicit to a certain bursting behavior, y is treated as bifurcation parameters of the fast-subsystem. This is formally correct in the singular system for $\epsilon = 0$, but is reasonable when there is large time separation between fast and slow dynamics. One should note that when $\epsilon \neq 0$, the existence of topological objects, such as equilibria and limit cycles, and events, such as bifurcations, of the *isolated* fast subsystem do not actually exist; they are merely estimates of system dynamics that converge to true dynamics as $\epsilon \to 0$.

An benefit of this fast-slow perturbation analysis is that it allows an objective categorization of bursting mechanism by the type of pseudo-bifurcation to and from the active phase. The Chay-Keizer model ref. [6] was the first single neuron model to report on intrinsic aperiodic spiking and bursting behavior ref. [1]. Using the topological categorization scheme, this model is a fold/homoclinic burster - it enters the spiking regime via a fold of equilibria and leaves when the stable periodic orbit describing spiking is annihilated via collision with an unstable equilibrium. The Chay-Keizer model is a five parameter model with four variables dictating fast dynamics

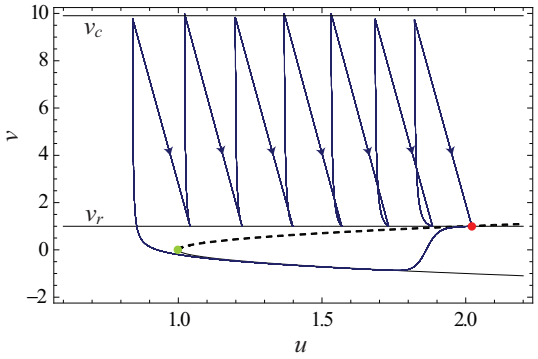

FIG. 1: Solution to (2) and (3) with parameters $I = 1, \mu = 0.02, v_c = 10, v_r = 1, d = 0.2$. With the exception of μ, these parameters are held constant in this report. v escapes from silence via fold of equilibria shown as a green dot. The stable equilibrium, v_{sq} (bold line) defines the resting potential during silence. After the fold, periodic spiking is enforced by resets, shown by lines with arrows, until $v_r = v_{uq}$ and v falls back to v_{sq} via a homoclinic orbit bifurcation, shown as a red dot.

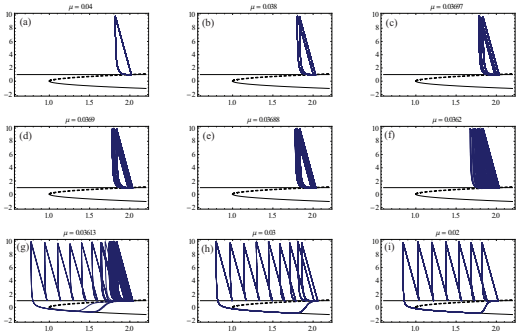

FIG. 2: Period doubling route to a chaotic regime in μ, as witnessed in the Chay-Keizer model, is confirmed in the canonical model.(a)-(e) period doubling route through 1-, 2-, 4-, 8-, 16-periodic solutions. (f) Aperiodic spiking. (g) Aperiodic bursting. (h,i) Stable bursting.

and a single slow variable. This system can be reduced to a canonical form while preserving the fold/homoclinic bursting mechanism. State equations are

$$\dot{v} = I + v^2 - u, \tag{3}$$

$$\dot{u} = -\mu u, \tag{4}$$

where I is a constant current and μ is a small positive constant. The system is reset after a voltage spike by,

$$\text{if } v = v_c, \ (v \leftarrow v_r, u \leftarrow u + d), \tag{5}$$

where $v_c - v_r$ and d are discrete shifts in variables that account for hyperpolarization and voltage coupling of u, respectively. Using the slow variable u as a bifurcation parameter of (3), the equilibria of v are $\sqrt{u - I}$. A topologically normal saddle-node bifurcation occurs at $u = I$. When $u < I$, $v \to v_c$ like $\tan(t)$ and a reset occurs. A typical bursting solution is plotted in Fig. 1.

III. ENTER CHAOS?

The Chay-Keizer model displays a regime aperiodic spiking in a parameter representing a time constant of the slow variable, equivalent to μ in (3). As the parameter corresponding to μ was decreased in their model, a transition from periodic spiking to bursting occurred via a period doubling sequence to a chaotic regime. We encounter the same behavior in our simplified model, as shown in Fig. 2.

IV. SYMBOLIC DYNAMICS

It is possible (and convenient) to further reduce (3–4) to a one dimensional discrete time map. To do this, we use a introduced by Lorenz in the examination of his attractor by recording spike to spike values of u. For $\mu = 0.0362$, this results in the mildly discouraging unimodal map shown in Fig. 3(a). We will refer to this map as the $U(u)$.

Iterated unimodal maps, like U, are well understood. The non-wandering set of U resides in $\mathcal{M} \approx [1.67204, 1.83674]$. $\mathcal{M}$ can be partitioned into two segments $\mathcal{M}_0 \approx [1.67204, 1.8)$, $\mathcal{M}_1 \approx (1.8, 1.83674]$ and a symbolic dynamics defined by

$$s_i = \begin{cases} 0 & \text{if } u_i \in \mathcal{M}_0 \\ 1 & \text{if } u_i \in \mathcal{M}_1. \end{cases} \tag{6}$$

Using (6), an infinite symbol sequence, $S^+(u_0) = s_1 s_2 s_3 ...$ represents a unique future itinerary for each $u_0 \in \mathcal{M}$. Kneading theory ref. [7] provides a simple way to relate U to a topologically-conjugate piecewise linear tent-map on the unit interval. A kneading sequence for U is $K = S^+(u_0^*)$ where $u_0^* = 1.80$ is the critical point that provides the maximum image under U. K is converted to the kneading point, $k_b^b = 0.w_1 w_2 w_3 ...$ by

$$w_{i+1} = \begin{cases} w_i & \text{if } s_{i+1} = 0 \\ 1 - wi & \text{if } s_{i+1} = 1, \end{cases} \tag{7}$$

where $w_1 = s_1$. Finally, k_b is converted to the kneading value k via a binary expansion. This value is then used to create the dike-map,

$$f(x) = \begin{cases} 2x & \text{if } x \in [0, k/2) \\ k & \text{if } x \in [k/2, 1 - k/2] \\ -2(1 - x) & \text{if } x \in (1 - k/2, 1]. \end{cases} \tag{8}$$

If one compares U with (7), it becomes apparent that if $f(S^+) > f(K)$ the the future itinerary S^+ is inadmissible in U since the image of the u_0 corresponding to S^+ exceeds u_0^*. With $\mu = 0.0362$, we estimated $k \approx 0.9147...$ for a finite K of 50 or so kneading segments to create the dike-map shown in Fig. 3.

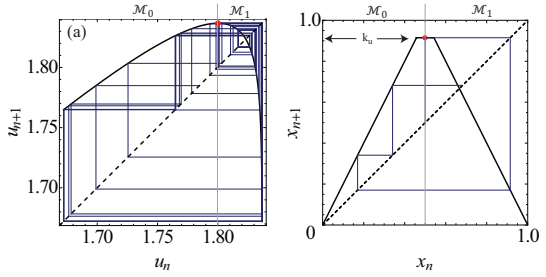

FIG. 3: (a) One-dimensional spike to spike map of u. State space is partitioned to allow a binary symbolic dynamics. The red dot is u_{crit} and therefore its images determine the kneading sequence allowing the creation of a topologically conjugate dike map. (b) The non-wandering set of the dike map is bounded between the kneading value k (arrow) and its image $-2k_u + 2$. The trajectory originating at the red dot has equivalent symbolic dynamics as the kneading trajectory in (a).

V. PRUNING AND CYCLE ID

Thus far, a biophysical neuron model has been reduced to a 2-dimensional canonical form and then to a 1-dimensional unimodal map. In order to elucidate qualitative properties of these equivalent systems using periodic orbit theory, we must locate periodic orbits. The first step in this process is to construct a grammar within the framework of the symbolic dynamics defined by (6) that excludes inadmissible periodic orbits.

Vis a vis symbolic dynamics, prime periodic points are a single representatives from the permutation class of each future itinerary that repeats after a finite length, $p_i = \overline{s_1 s_2 ... s_n} = \overline{s_n s_1 ... s_{n-1}} = \cdots = \overline{s_2 s_3 ... s_1}$. By identifying inadmissible symbol strings, called *pruning blocks*, under f and removing periodic itineraries that contain these blocks from the set of full binary prime cycles, we determine what cycles are admissible under U. Pruning blocks are identified by the following pruning rule: any string of adjacent symbols that results in an image of f greater than k cannot exist under U.

There exist and infinite number of pruning blocks for f. Their identities are revealed by examining the succession of images of k shown in Fig. 3(b). One pruning block is obvious from the figure: no more than two adjacent 0's can appear in an itinerary of the non-wandering set. Thus, _000_ is a pruning block of f. To find the rest, notice that K begins with two 0's and then is mapped to $u < u_q = 2/3$ where u_q is the fixed point corresponding the the fixed point $\overline{1}$. One can deduce from this that any itinerary with adjacent 0's will map to $\{u \in \mathcal{M}_1 | u < u_q\}$. Because of this, as the itinerary progresses, it forms a clockwise cobweb around u_q and in this case,

$$f \ : \ \{u \in \mathcal{M}_1 | u < u_q\} \mapsto \{u \in \mathcal{M}_1\} \quad (9)$$

$$f \ : \ \{u \in \mathcal{M}_1 | u > u_q\} \mapsto \{u \in \mathcal{M}_0 \cup \mathcal{M}_1\}. \quad (10)$$

Hence, the itinerary must leave $\mathcal{M}_1$ from a $u > u_q$ but enters at a $u < u_q$. An equivalent statement is: subsequences $\_00S_x0\_$ with $S_x = \{11, 1111, 111111, ...\}$ comprise an infinity of pruning blocks for f (Fig. 5(a)).

TABLE I: Admissible prime cycles of U.

Length	Cycle	Length	Cycle	Length	Cycle
1	1	2	01	3	001 011
4	0111	5	00101 00111 01011 01111	6	001011 010111 011111
7	0010101 0010111 0011111 0100111 0101111 0110111 0101011 0111111	8	00100101 00100111 00101011 00101101 00101111 00111011 01010111 01011011 01011111 01101111 01111111	9	001001011 001010101 001010111 001011011 001011101 001011111 001110101 001110111 010101011 010101111 010110111 010111011 010111111 011011111 011101111 011111111

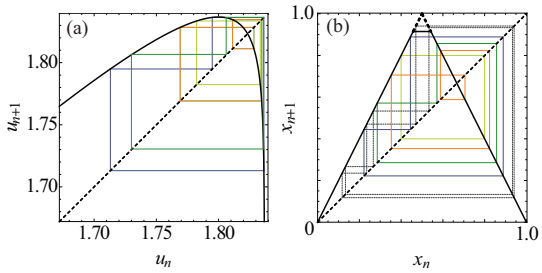

FIG. 4: (a) Prime cycles of U to length 4. (b) Equivalent prime cycles found of f. Pruning blocks _000_ and _0011_ disallow $\overline{0001}$, and $\overline{0011}$. These are shown as black lines; notice how they violate the kneading condition by producing images greater than k.

Prime cycles are identified as repeating binary symbol strings that do not contain a pruning block and are given in Table I to length 9. Armed with this information, finding cycle points under U is simple given an adequate search method. We implemented a multi-point shooting routine ref. [8] to find cycle points on U, the first few results of which are shown in Fig. 4.

VI. TRANSITION GRAPH

A compact description of all admissible itineraries under U is represented by walks on an infinitely large Markov-graph that conforms to the previously defined grammar. This graph is infinitely large to accommodate the infinite pruning blocks defined above, but finite truncations will be useful for practical calculation. For example, Fig. 5(b,c) shows the formation of a Markov-graph

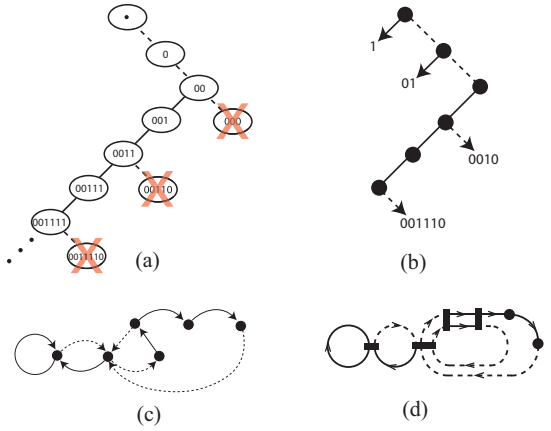

FIG. 5: The construction of a finite transition graph and shadowing graph for f and/or U. Solid lines represent ones and dashed lines zeros. This example is trucated to include the pruning blocks _000_ and _00110_. (a) First a binary path to all pruning blocks is diagramed. (b) Next, admissible continuations are provided with arrows. (c) The transition graph is finished by finding where these continuations "feed back into" the diagram. Symbols on the continuations are removed from the left until a match to a node in (a) is found, then a recurrent connection is created. (d) A shadowing graph is created by delineating intersection points for loops of (b) on the same graph.

for itineraries under U of length 6 or less. Periodic orbits are represented by walks that return to their starting point on the graph.

T is the transition matrix that accounts for all possible transitions on Fig. 5(c) and is given by the following [6×6] matrix.

$$T = \begin{pmatrix} 1 & 1 & 0 & 0 & 0 & 0 \\ 1 & 0 & 1 & 0 & 0 & 0 \\ 0 & 0 & 0 & 1 & 0 & 0 \\ 0 & 1 & 0 & 0 & 1 & 0 \\ 0 & 0 & 0 & 0 & 0 & 1 \\ 0 & 1 & 0 & 0 & 0 & 0 \end{pmatrix}$$

VII. TOPOLOGICAL ENTROPY

Figure 5(c) can be transformed into the shadowing graph in Fig. 5(d) by simultaneously graphing all *non-intersecting loops* of the transition graph ref. [8]. The characteristic polynomial of a finite graph is given by the sum of all possible partitions, π, of the graph into products of k non-intersecting loops, t_p each loop trace carrying a minus sign ref. [8],

$$\det(1 - zT) = \sum_k \sum_\pi (-1)^k t_{p1} \dots t_{pk}. \tag{11}$$

Since our transition graph is infinite, the identity above must be approximated via a cumulate expansion ref. [8],

$$\begin{aligned} \det(1 - zT) &= 1/\zeta_{top} \\ &= \prod_p (1 - z^{n_p}) \qquad (12) \\ &= 1 - \sum_{n=1}^{\infty} c_n z^{n_p}. \qquad (13) \end{aligned}$$

This formula is known as the *topological zeta function*. For the purpose of calculating the topological entropy, we set the cumulant expansion coefficients, $c_n = 1$ and the weight of a prime cycle p to $t_p = z^{n_p}$ if p exists and $t_p = 0$ if it is pruned. Thus a finite estimate of the topological zeta function for Fig. 5(c) can be read off the shadowing graph, which shows fundamental loops. It is,

$$\begin{aligned} 1/\zeta_{top} &= 1 - t_1 - t_{01} - t_{001} - t_{00111} + \\ &\quad t_1 t_{001} + t_1 t_{00111} \\ &= 1 - z - z^2 - z^3 + z^4 - z^5 + z^6. \end{aligned} \tag{14}$$

The smallest real zero of this approximate topological zeta function is $z = 0.569840...$ giving topological entropy

$$h = -\ln(0.569840...) = 0.562399... \tag{15}$$

The transition matrix, T, for our finite transition graph can be used to check if the zeta function is correct. The leading eigenvalue of this matrix is $\lambda_\circ = 1.75488....$ The topological entropy

$$h = \ln(1.75488...) = 0.562399..., \tag{16}$$

copies the zeta function result.

VIII. DENSITY TRANSPORT

The following is a brief outline of material detailed in ref. [8] that will motivate the following paragraphs. Let $\rho(u, n)$ be a function defining a density over the non-wandering set of U, Ω, with infinite partition $\Omega = \{\mathcal{M}_1, \mathcal{M}_2, \dots\}$. $\rho(u, n)$ has normalization

$$\int_\Omega \rho(u, n) du = 1. \tag{17}$$

We can define a linear operator $\mathcal{L}^n$ that acts on the space of real analytic functions (that can define $\rho(u, n)$) called the *Perron-Frobrenius operator (PFO)*. For the U, $\mathcal{L}^n$ can be thought of as an infinitely large square matrix linearly transforming initial densities of points in each infinitesimal partition of state-space. Periodic orbit theory provides an elegant method to relate the eigenspectrum of $\mathcal{L}^n$ to periodic orbits under U in order to measure average quantities of a chaotic system.

In an unstable system, prediction of specific dynamics is impossible since initial conditions can only be specified to finite precision. Finding long time averages of

over chaotic dynamics is, however, possible and made exponentially accurate in practice via implementation of periodic orbit theory. Let a be some observable we are interested in. We can integrate this observable over a prime cycle p of length n_p of with cycle point u_0,

$$A_p(n) = \sum_{i=1}^{n_p} a(f^n(u_0)). \tag{18}$$

Since the prime cycles of a chaotic system are areas of high recurrence and since the flow is assumed to be smooth and hyperbolic, the crux of periodic orbit theory states that long time averages of observables for a chaotic systems can be represented by weighted sums of observables on periodic orbits ref. [8]. This idea is intuitive: the calculation of observables on periodic orbits can be carried out in finite time since in infinite time, the orbit contributes only multiples, kA_P, of the observable integrated over a single period.

If we continue to think of $\mathcal{L}^n$ as a square matrix, it is easy to visualize how $\mathrm{tr}\,\mathcal{L}^n$ relates to periodic orbits. Entries along the diagonal of $\mathcal{L}^n$ operate to cause a recurrence of $p(u,n)$ in time. As $n \to \infty$ the action of $\mathcal{L}^n$ is dominated by its leading eigenvalue. Since,

$$\mathrm{tr}\,\mathcal{L}^n = \sum \mathrm{eig}(\mathcal{L}^n), \tag{19}$$

$\mathrm{tr}\,\mathcal{L}^n$ is dominated by the leading eigenvalue as well. The specific method for determination of the spectrum of $\mathcal{L}^n$ from periodic orbits is fully explained in ref. [8]. We now implement this idea for the U map in order to determine whether the system is in fact chaotic.

IX. WHAT IS CHAOS?

Chaotic dynamics are defined by two qualities: orbits are (1) locally unstable yet (2) global recurrent (mixing). We have already shown that dynamics under U fulfill the second characteristic. Topological entropy is the rate of increase in the number of admissible periodic orbits with respect to cycle length. Since U has a positive topological entropy, individual trajectories show an increasing tendency for recurrence over long time evolution.

One way to show that the dynamics under U is chaotic, is by calculating its *Lyapunov exponent*

$$\lambda = \lim_{n\to\infty} \frac{1}{n} \ln |\delta u(n)|/|\delta u_0|, \tag{20}$$

where δ is a small separation between two initial conditions. Thus the Lyapunov exponent describes the mean rate of separation between trajectories in a given system, $|\delta x(t)| = e^{\lambda t}|\delta x_0|$. If the Lyapunov exponent of U is positive, then the system is chaotic since both criteria for chaos are fulfilled.

X. CYCLE EXPANSIONS FOR DYNAMICAL AVERAGING

Zeta functions can be respresented as a series of of unstable periodic orbits of increasing length appropriately weighted by instability, length and their integrated observable called a *cycle expansion*,

$$1/\zeta = \sum_{\mathrm{fund}} t_{\mathrm{fund}} - \sum_n c_n, \tag{21}$$

where first sum is over fundamental cycles and the second term is a sum over curvature corrections. Fundamental cycles are those that cannot be shadowed by pseudocyles composed of combinations of extant prime cycles. The curvature parts are prime cycles minus their shadowing pseudocycles, which makes these corrections small. Zeros of cycle expansions give the eigenvalues of the evolution operator. If all cycles are weighted equally, this formula reduces to the topological zeta function (14). The cycle expansion of U to length 6 is given by,

$$\begin{aligned}
&1/\zeta = 1 - t_1 - t_{01} - t_{001} - [(t_{011} - t_{01}t_1)] \\
&-[(t_{0111} - t_{011}t_1)] - [(t_{00101} - t_{001}t_{01}) + \\
&t_{00111} + (t_{01011} - t_{01}t_{011}) + \\
&(t_{01111} - t_{0111}t_1)] - [(t_{001011} - t_{001}t_{011} - t_{00101}t_1 + \\
&t_{001}t_{01}t_1) + (t_{010111} - t_{01}t_{0111} - t_{01011}t_1 + t_{01}t_{011}t_1) \\
&+(t_{011111} - t_{01111}t_1)] - \ldots
\end{aligned} \tag{22}$$

The weight of a cycle within the cycle expansion (22) is given by,

$$t_\pi = (-1)^{k+1} \frac{1}{\Lambda_\pi} e^{\beta A_\pi - sT_\pi} z^{n_\pi}, \tag{23}$$

where A_π is some observable integrated over the cycle or pseudocycle cycle, π, of length n_π and stability Λ_π. When calculating observable on non-dissipative systems, the leading eigenvalue of $\mathcal{L}^n$, equivalent to the leading zero of (12), acting on the space of real analytic functions is $z_\circ$=1. Thus ρn is conserved under $\mathcal{L}^n$; the escape rate is 0.

The derivative of the dynamical zeta function evaluated at an appropriate eigenvalue provide exponentially converging estimates of dynamical averages in increasing expansion length. For bounded flows, where the leading eigenvalue of the evolution generator is $s = 0$, the exponent in (23) vanishes and this derivative reduces to

$$\langle A \rangle_\zeta = \sum_\pi (-1)^{k+1} \frac{|A_{p1}| + |A_{p2}| + \cdots + |A_{pk}|}{|\Lambda_{p1} \ldots \Lambda_{pk}|}. \tag{24}$$

Therefore, the Lyapunov exponent can be evaluated as

$$\lambda_\zeta = \frac{1}{\langle n \rangle_\zeta} \sum_\pi (-1)^{k+1} \frac{\ln|\Lambda_{p1}| + \cdots + \ln|\Lambda_{pk}|}{|\Lambda_{p1} \ldots \Lambda_{pk}|}, \tag{25}$$

where $\langle n \rangle_\zeta$ is calculated by (24).

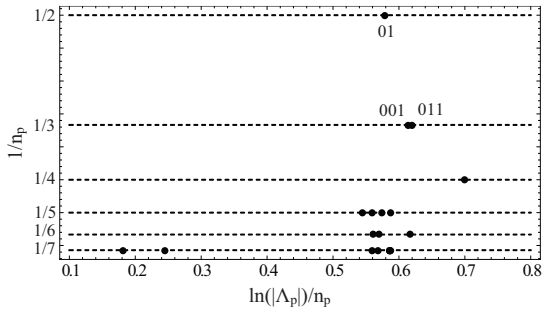

FIG. 6: Lyapunov exponents for prime cycles to length seven shown against the inverse of cycle length. Note that at two prime cycles of length seven, $\overline{0011111}$ and $\overline{0100111}$, have Lyapunov exponents near marginal. This occurs because these orbits contain cycle point very close to u_0^* and this should make us reconsider there use in the expansion.

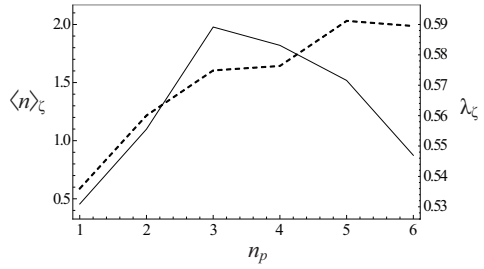

FIG. 7: Cycle averages for $\langle n\rangle_\zeta$ (dashed) and λ_ζ (solid). After $n = 5$, all fundamental cycles have contributed to the expansion, and only small curvature corrections polish the estimate. If the cycle expansion were carried out for longer cycles, this would be more obvious.

It is important to note that this method only works for systems that are strictly hyperbolic; that is they are are exponentially bounded away from marginal stability, $\lambda = 0$. The Lyapunov exponent for prime cycles to length seven are shown in Fig. 6. The system is hyperbolic, but at some cycles are close to marginal stability which implies the convergence of dynamical averages may be slow in cycle length.

The estimate of the Lyapunov exponent by the cycle averaging formula (25) is given for finite cycle expansion truncations to length 6 in Fig. 7. Because we only carried out the calculation for cycles to length 6, the convergence of the estimate is not obvious. However, this is to be expected as shown in refs. [9, 10]. Since (22) accounts for all fundamental cycles, the the basic estimate of λ_ζ to after length 5 should be generally accurate. If we had continued the calculation for longer cycles, the estimate would have fully converged. We obtained a final estimate of $\lambda_\zeta = 0.54695$.

XI. LYAPUNOV EXPONENT THE EASY WAY

A common way to calculate the Lyapunov exponent of a one dimensional map is by a Taylor expansion to linear order,

$$\delta u_{i+1} = \frac{\mathrm{d}U}{\mathrm{d}u}\delta u_i + \dots \tag{26}$$

Therefore, a local Lyapunov exponent is defined by

$$\lambda_{loc} = \log|\frac{\delta u_{i+1}}{\delta u_i}| = \log|\mathrm{D}U|. \tag{27}$$

This calculated many times over a trajectory and averaged to get an estimate of λ. By averaging λ_{loc} for 10,000 iterations, we estimated $\lambda = 0.536377$ which confirms general accuracy of the cycle averages (22).

XII. DISCUSSION

We have shown that the fold/homoclinic bursting neuron investigated by Chay *et. al.* ref. [1, 6] is chaotic over a narrow region of parameter space corresponding to a recovery time constant for some slow variable u. The fact that the chaotic regime of μ was narrow is totally general to all single slow variable bursting neurons. To understand why, we return to the state-space analysis presented at the beginning of this report.

Chaos in single slow variable bursting neurons can only occur when the singular perturbation methods described in sect. II fail to provide an accurate description bursting dynamics. Fig. 8 is a magnification of Fig. 2(f). If the fast and slow dynamics were infinitely separated in time in the dotted line representing the unstable equilibria would provide a definitive saddle point for trajectories to maintain a limit cycle in the fast subsystem or contract to its fixed point after the homoclinic orbit bifurcation. This is not true in the chaotic regime. Instead each trajectory is rides close to the unstable manifold of this pseudo-saddle for sometime before quickly diverging back to the pseudo-limit cycle of the fast subsystem. This action provides the local instability (stretch) and the discrete resets provide the recurrence (fold). If the fast-slow separation was accurate, all trajectories would converge on the equilibrium of the fast subsystem and all local instability would be lost, resulting in the stable bursting limit cycles seen for low values of μ. Hence, chaotic spiking in a single neuron with one slow variable necessary occurs 'briefly' at the transition between tonic spiking and bursting.

In terms of biological neural systems, it is obvious why this mode of chaotic activity in a single neuron is probably not very meaningful. The large noise present in even the simplest of nervous systems make it unlikely a phenomenon relying on such a fragile choice of parameter would be useful. Additionally, the idealization studied in this report is a single neuron, in total synaptic isolation. A functional neuron is constantly barraged my

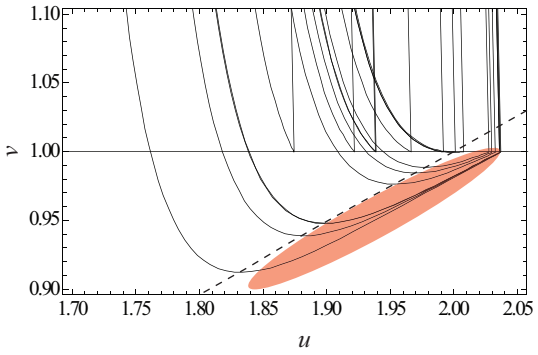

FIG. 8: Magnification of Fig. 2(f). The local instability of the chaotic fold/homoclinic bursting is equivalent to the failure of fast/slow dissection techniques. Instead of the unstable equilibria of the fast subsystem, shown as a dotted line, being hard boundary for trajectories to continue spiking or return to rest, it provides the local instability needed for chaotic dynamics to emerge (red portion of state-space). Recurrence to this area of instability is provided by the discrete resets, or in biology by hyperpolarization following each action potential.

many inputs that commonly have some effect on parameters such as the recovery time constant of a slow chemical oscillation, like those of calcium currents, hyperpolarization activated currents, and slow sodium currents. As was stated at the beginning of this report: it is absurd to think of a highly coupled system of non-linear oscillators, like a biological neural network, without considering chaotic dynamics. However in the case of an isolated one-variable bursting neuron, it seems unlikely for chaos to more than an interesting epiphenomenon.

[1] T. Chay and J. Rinzel, Biophys. J. **47**, 357 (1985).
[2] A. B. V. Matveev and F. Nadim, J. Comput. Neurosci. **23**, 169 (2007).
[3] Y. Chagnac-Amitai and B. Conner, J. Neurophysiol. **62**, 1149 (1989).
[4] R. Butera, J. Rinzel, and J.C.Smith, J. Neurophysiol. **81**, 382 (1999).
[5] R. Plant and M. Kim, Biophys. J. **16**, 227 (1976).
[6] T. Chay and J. Keizer, Biophys. J. **42**, 181 (1983).
[7] P. Collet and J. Eckmann, Iterated Maps on the Interval as Dynamical Systems (Birkhauser, Boston, 1980).
[8] P. Cvitanović, R. Artuso, R. Mainieri, G. Tanner, and G. Vattay, Chaos: Classical and Quantum (Niels Bohr Institute, Copenhagen, 2008), `ChaosBook.org`.
[9] R. Artuso, E. Aurell, and P. Cvitanović, Nonlinearity **3**, 325 (1990).
[10] R. Artuso, E. Aurell, and P. Cvitanović, Nonlinearity **3**, 361 (1990).